

3D Analysis of Amorphous Polymers Deformation under Mode I

Shu Guo^{1,2}, Rafael Estevez^{2,*}, Sabine Weygand³, Christian Olagnon¹

¹ MATEIS, INSA Lyon, 69621, France

² SIMAP, Université de Grenoble, 38401, France

³ University of Applied Science, HS Karlsruhe, 76133, Karlsruhe, Germany

* Corresponding author: Rafael.Estevez@simap.grenoble-inp.fr

Abstract Fracture in ductile glassy polymers is usually preceded by noticeable and extensive plastic deformation, as shear yielding takes place in the form of shear bands that are limited by progressive hardening of materials at continuous deformation. In the case of a notched specimen, this induces a noticeable crack blunting before the failure. We use a constitutive law that captures realistically the stress-strain fields of solid glassy polymers. In particular, we account for a rate dependent yield stress followed by intrinsic softening and progressive hardening at continued deformation. We analyzed the 3D crack tip fields around a blunted notch loaded under mode I. With an increasing ratio between thickness versus notch tip radius, the shape of crack tip area evolves from a flame like zone characteristic of plane stress conditions to slip lines when plane strain conditions prevail. For a constitutive law representing the response of polycarbonate, we identified a critical thickness vs notch radius value that indicates the transition between plane stress to plane strain dominant loading conditions. The implication for the geometry necessary to derive material toughness experimentally is pointed out and an examination of the mean stress constraint related to the onset of failure by crazing is reported.

Keywords crack tip plasticity, fracture, glassy polymers, 3D effects

1. Introduction

Fracture in glassy polymer involves the competition between two localized plastic deformation: shear yielding and crazing. Shear yielding is related to the material's mechanical response with the localization of plastic deformation upon yielding followed by progressive hardening that controls the shear bands thickness. Crazing is the mechanism underlying failure that involves also localized plasticity, although at a much smaller scale. In glassy polymers, the crack tip fields around a notch loaded under mode I have been analyzed in a seminal paper by Lai and Van der Giessen [1] for 2D plane strain condition. These authors showed that the specific plastic zone made of a collection of shear bands similar to Hill's slip lines is related to the material's constitutive law with softening triggering the formation of shear bands of which development is arrested by progressive hardening at continued deformation. This latter feature acts as a shear bands lock that promotes the nucleation of new shear bands to form a specific plastic zone; in the case of thin polymer films, when plane stress conditions prevail, a flame like plastic zone is observed, for instance in tests by the essential work of fracture (EWF) tests [2]. In ductile polymer fracture, when the onset of failure is preceded by noticeable plastic deformation as in polycarbonate, to determine the geometry for which plane strain conditions prevail remains heuristic from an experimental point of view. For instance, Parvin and Williams [3] observed that a ductile to brittle fracture transition takes place in a SENT polycarbonate specimen with increasing the sample's thickness. They ascribed this transition to a critical thickness (t) versus size of the plastic zone (r_p) as t/r_p , with r_p the extent of plastic zone under plane stress condition. By taking K_{c1} the toughness measured for thick samples and K_{c2} that for thin samples, they proposed an empirical relationship that captures the variation on the toughness with the specimen's thickness. More recently, Tvergaard and Needleman [4] investigated the

thickness effects in Izod fracture tests used in polymer samples and pointed out differences in the crack tip fields. For the thicker specimens, the predicted maximum mean stress appears much higher in the midsection than on the free surface. For thin specimens, a similar mean stress constraint is observed across the material's thickness, which indicates that plane stress conditions prevail. For the measure of the material's toughness, one wished to ensure that plane strain conditions prevail and if not, to estimate whether plane stress or a combination between plane stress and plane strain conditions is met. We present an analysis of the crack tip fields along the spirit of Lai and Van der Giessen [1] but within a 3D framework. The results presented here show that the shape of the predicted plastic zone can be used as an indicator of the plane stress/ plane strain condition and a geometrical criterion is proposed for the estimation of the thickness large enough to ensure plane strain conditions.

The paper is organized as follows. We first present the materials constitutive law and report the parameters identified for the polycarbonate under consideration. Then we present the 3D notched configuration and related problem formulation. For identical loading conditions, the influence of the thickness on the predicted crack tip fields in terms of cumulated plastic deformation is reported. The analysis of the variation of the mean stress with thickness, and its comparison with 2D calculations performed for plane stress and plane strain conditions are presented and used for proposing a criterion indicating when plane strain conditions prevail.

2. Material model and parameters identification

2.1. Constitutive Law

The constitutive law used to model the large strain plastic behavior is based on original ideas due to Boyce et al. [5] with some modifications introduced later by Wu and Van der Giessen [6] for the hardening part. In this section, we report the governing equations and materials parameters to be identified to represent the bulk, craze-free, response. The reader is referred to [7] for details on the computational aspects. The 3D constitutive model has been implemented in abaqus [8] within a User Material routine. The mechanics of fully three-dimensional large strain deformation involves the deformation gradient tensor F , which maps a material point of the reference configuration into the current configuration. The deformation gradient is multiplicatively decomposed as $F = F^e F^p$, in which F^p describes the deformation from the initial to an intermediate, "relaxed" or "natural" configuration, followed by an elastic transformation F^e up to the final deformation F . The velocity gradient in the current configuration is $L = \dot{F}F^{-1} = \dot{F}^e F^{-e} + F^e \dot{F}^p F^{-p} F^{-e}$ of which symmetric and anti-symmetric part correspond to the strain rate and spin tensor, D and W respectively. When the elastic part F^e of the deformation gradient is small compared to the plastic one F^p (i.e. $F^e \approx I$), the velocity gradient reduces to $L = L^e + L^p$ so that the total strain rate D becomes the sum of the elastic and plastic parts as $D = D^e + D^p$.

Prior to the yield stress, amorphous glassy polymers exhibit a non linear stress strain response due to small viscoelastic effects. These are not considered explicitly but their effect on the mechanical response is accounted for by using a secant Young modulus instead of that derived from ultra-sonic wave velocities. In view of these approximations, the hypo-elastic law is used to express the bulk mechanical response as

$$\overset{\nabla}{\sigma} = L_e D^e, \quad (1)$$

where $\overset{\nabla}{\boldsymbol{\sigma}}$ is the Jaumann rate of the Cauchy stress, \mathbf{L}_e the fourth-order isotropic elastic tensor in terms of secant Young modulus E^{SECANT} and Poisson's ratio ν , which is in Cartesian components $L_{ijkl} = \frac{E}{2(1+\nu)} \left[(\delta_{ik}\delta_{jl} + \delta_{il}\delta_{jk}) + \frac{2\nu}{1-2\nu} \delta_{ij}\delta_{kl} \right]$.

Within the elastic-viscoplastic framework used here, the plastic strain rate is

$$\mathbf{D}^P = \mathfrak{K} \frac{\bar{\boldsymbol{\sigma}}'}{\sqrt{2\tau}}, \text{ with } \tau = \sqrt{\frac{1}{2} \bar{\boldsymbol{\sigma}}' \cdot \bar{\boldsymbol{\sigma}}'} \quad (2)$$

being the equivalent shear stress and $\bar{\boldsymbol{\sigma}}$ the deviatoric part of the driving stress. The driving stress itself is defined by $\bar{\boldsymbol{\sigma}} = \boldsymbol{\sigma} - \mathbf{b}$. The back stress \mathbf{b} responsible for the hardening is due to the entropic back forces generated by the deformation of the polymer chains during the plastic deformation, and will be defined later. The equivalent plastic shear rate \mathfrak{K} is taken according to Argon's [9] expression

$$\mathfrak{K} = \mathfrak{K}_0 \exp\left[-\frac{A(s_0 + \alpha p)}{T} \left(1 - \left(\frac{\tau}{s_0 + \alpha p}\right)^{5/6}\right)\right], \quad (3)$$

where \mathfrak{K}_0 and A are material parameters and T is the absolute temperature. Following Boyce et al. [5], intrinsic softening is accounted for with the definition of an internal variable s which varies from s_0 to s_{ss} at continued plastic deformation. The internal law

$$\mathfrak{K} = h(1 - s/s_{ss})\mathfrak{K}_0 \quad (4)$$

governs its variation during deformation, with h a parameter controlling the rate of softening and s_{ss} the value of s in a steady state regime. Furthermore, Equation (3) is modified in order to account for the pressure dependence by using $s + \alpha p$ instead of s_0 in (3), where $-p = 1/3 \text{tr}\boldsymbol{\sigma}$ is the mean (or hydrostatic) stress. The coefficient α represents the pressure sensitivity of the polymer which results in an asymmetric yield stress in tension and compression, for instance.

The description for back stress tensor \mathbf{b} is based on ideas borrowed from theories for rubber elasticity with the cross-links of the rubbers considered as "entanglements" in the case of glassy polymers. The deformation of the resulting network is assumed to derive from the cumulated plastic stretch so that the principal back stress components b_α are functions of the principal plastic stretches λ_β as

$$\mathbf{b} = \sum_\alpha b_\alpha \left(\mathbf{e}_\alpha^p \otimes \mathbf{e}_\alpha^p \right), \quad (6)$$

in which \mathbf{e}_α^p are the principal directions of the plastic stretch. In a description of the fully three-dimensional orientation distribution of non-Gaussian molecular chains in a network, Wu and Van der Giessen [10] showed that \mathbf{b} can be estimated accurately with the following combination of the classical three-chain model and the eight-chain description of Arruda and Boyce [11]

$$\mathbf{b} = (1 - \rho)\mathbf{b}^{3\text{-ch}} + \rho\mathbf{b}^{8\text{-ch}}, \quad (7)$$

where the fraction $\rho = 0.85\bar{\lambda}/\sqrt{N}$ is based on the maximum plastic stretch $\bar{\lambda} = \max(\lambda_1, \lambda_2, \lambda_3)$ and on N , the number of segments between entanglements. The use of Langevin statistics for calculating b_α

implies a limit stretch of \sqrt{N} . The expressions for the principal components of b^{3-ch} and b^{8-ch} contain a second material parameter: the initial shear modulus $C^R = nk_B T$, in which n is the volume density of entanglements (k_B is the Boltzmann constant).

2.2. Parameters identification

In order to obtain a set of material parameters for the description of the finite strain visco-plastic response of the polycarbonate under consideration, experimental data of the stress-strain response for various strain rates are necessary. In compression, crazing is suppressed and uniaxial experiments are carried out on cylindrical specimens. In order to prevent any buckling, the diameter and the height of the specimen are 10 mm and 6 mm respectively. Low friction along the contact surface between the faces of the cylinder and the plates of the machine is ensured by using a hexagonal boron nitride powder (BN). Therefore, lateral displacement with respect to the direction of compression is allowed so that a uniform stress state prevails along the whole specimen. In order to characterize the rate dependency of the yield stress, a series of strain rates from $1 \times 10^{-5}/s$ to $1 \times 10^{-1}/s$ are investigated (see Fig. 1(a)). Following the identification procedure detailed in Saad et al., [12], the parameters are extracted from the uniaxial compression data and are reported in Table 1. The corresponding predictions are presented in Fig. 1(b).

Table 1. Material parameters for Polycarbonate

E^{sec} (MPa)	ν	s_0 (MPa)	s_{ss} (MPa)	α	A (K/MPa)	h (MPa)	$\dot{\gamma}_0$ (s^{-1})	C^R (MPa)	N
1300	0.39	88	68	0.08	195	450	$9.2e09$	17	3

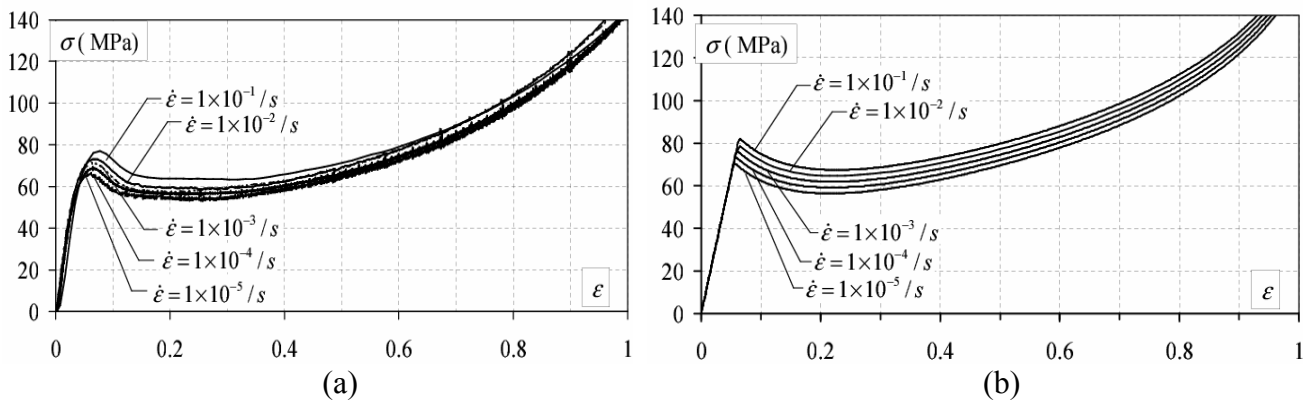


Figure 1. (a) Experimental cylinder compression stress-strain curves at strain rates varying from $1 \times 10^{-5}/s$ to $1 \times 10^{-1}/s$ (b) Predicted stress-strain response with the parameters identified in Table 1.

3. Problem formulation

In this section, we present the geometry of the specimen under consideration and the mesh used for the finite element analysis.

3.1. 3D analysis of a notched specimen under tension

The full 3D geometry of standard specimen loaded under mode I has dimension of $h=40$ mm, $w=20$ mm and $a=10$ mm, with a variable thickness B (see Fig. 2, left side). A blunted notch of radii $R=0.25$ mm is considered. We use a blunted notch that would correspond to the blunting of a sharp crack up to this magnitude. It is also motivated by experimental issues in which practically machining a sharp notch is difficult if not impossible experimentally. The preparation of a blunted notch is preferred for the fracture measurements to be reproducible. The constitutive law described in section 2 is implemented in a UMAT subroutine in abaqus 6.10-2 [8] and used.

3.2. Description of the mesh

The geometry and the mesh are presented in Fig. 2. Refined elements are used around the notch to capture the stress-strain fields. In the region remote to the notch area coarser elements are used. The elements consist in C3D20R, which is a 20-node quadratic brick, with reduced integration. The amount of elements across the thickness is increased with the thickness increasing, their dimension remaining identical. For instance with $R=0.25$ mm and thickness $t=1$ mm, the mesh comprises of 12 layers of elements through the thickness of the specimen; a total number of 15558 quadratic elements and 70574 nodes are employed. The smallest element has an edge of 0.0027mm. A constant displacement rate $\dot{u}=5$ mm/s is prescribed on the top surface to mimic a Single Edge Notch Tension for all calculations.

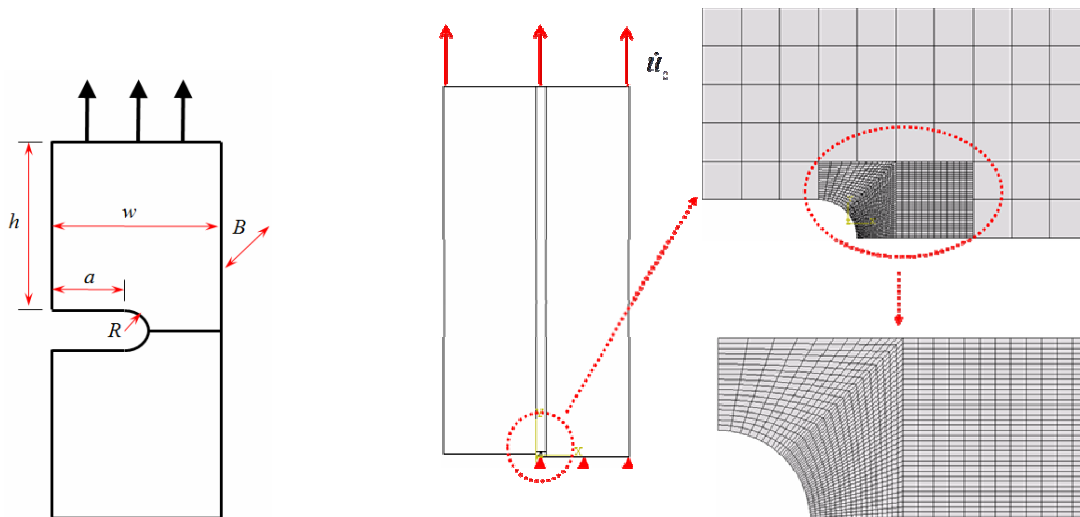


Figure 2. Geometry and mesh description for the Single Edge Notch Tension configuration

4. Results

In this section, we investigate the influence of the thickness on crack tip fields of blunt-notched specimens (see section 4.1.), with notch radius $R=0.25\text{mm}$. During the loading, plasticity initiates at the notch tip and extends on the notch region. The distribution of accumulated plastic shear strain around the notch is reported in Fig. 3. The variation of the maximum mean stress with the loading history represented by the overall axial strain $E_{\text{axial}}=u/2h$ is presented next.

4.1. Influence of the thickness on crack tip plasticity

Three sets of plastic shear strain distributions, and related contours, are reported in Fig. 5(a)-(i) at various load levels in terms of axial strain E_{axial} , for specimen thickness $t=0.25\text{ mm}, 1\text{ mm}$ and 4 mm , respectively.

For the thickness $t=0.25\text{ mm}$ ($t/R=1$), we present in Fig. 3(a-c) the plastic shear strain distribution at the onset of plasticity(see Fig. 3(a)) and continued deformation(see Fig. 3(b) and 3(c))on the surface as well as at the center of the specimen. Far from the notch, no plasticity takes place and the response is elastic. Around the notch, we observe that the plastic zone initiates and grows simultaneously at the surface and in the center of the specimen, but the shape of the plastic zone is different. At $E_{\text{axial}}=0.75\%$ it is seen that certain amount of plasticity arises around notch tip(see Fig. 3(a)). A homogeneous plastic zone inclined -30° from the equator is observed at the center, whereas a bifurcated plastic zone appears on the surface. With ongoing deformation, plastic zones both inside and outward expand rapidly. In Fig. 3(b), as E_{axial} equals to 0.875% , the plastic zone at the center gets a flame-like profile. At the surface, the plastic zone expands into a flame-like elongated plastic zone as well, which grows nearly parallel to the equator. Finally, as indicated in Fig. 3(c), a larger elongated plastic zone along the equator is observed at the center, whereas a similar elongated plastic zone appears parallel to the equator on the surface. For the configuration with thickness $t=1\text{ mm}$ ($t/R=4$), at $E_{\text{axial}}=0.75\%$, plasticity initiates with very small amount of plasticity on the surface, and in the form of tiny shear bands at the center(see Fig. 3(d)). For E_{axial} about 0.875% , plasticity areas do not proceed much both inside and outward(see Fig. 3(e)), as compared with Fig. 3(b). Finally, instead of forming a flame-like elongated plastic zone as the $t/R=1$ case, a circular-arc shaped plastic zone concentrated near the crack tip at the center(see Fig. 3(f)). Thus, the plastic zone appears different for $t/R=1$ and $t/R=4$ till now. If the thickness of specimen is further increased to $t=4\text{ mm}$ ($t/R=16$), in Fig. 3(g), when plasticity initiates at $E_{\text{axial}}=0.75\%$, clear shear bands arise around the notch in the center, whereas on the surface only a tiny area of plasticity is observed. As $E_{\text{axial}}=0.875\%$, shear bands continued to widen and diffuse at the mid-thickness, on the other hand, still tiny amount of plasticity exists on the surface (see Fig. 3(h)). With E_{axial} up to 1.125% , plastic deformation on the surface is still confined in a tiny region, whereas shear bands at the center enlarge a lot within a circular-arc, as shown in Fig. 3(i). This observation is similar to the plastic zone reported by Lai and Van der Giessen [1].

For the thinner specimen considered with thickness $t=1\text{mm}$ ($t/R=1$), we observe that the magnitude of plastic zone at the center is comparable to that on the surface, which rationalize the fact that the plane stress conditions prevail. In the case of $t/R=4$, the plastic zones appear significantly less elongated when compared to the case with $t/R=1$, both in the middle of the thickness and at the

surface for the same overall deformation. Besides, the plastic strain distribution at the center is no longer comparable to that on the surface as in Fig. 3(a)-(c). This phenomena that plasticity on the surface failed to proceed as much as that at the center(see Fig. 3(d)-(f)) represents a transition from plane stress to plane strain conditions within the material. Finally, for the thick specimen with $t/R=16$ (thickness of 4mm), the apparent discrepancy in the shape of locally deformed area at the mid-thickness and on the surface indicates that plane strain condition dominates in the specimen.

The shape of the plastic zone corresponding to a flame-like profile under plane stress condition(see Fig. 3(c)), is found to agree well with Hashemi's [2] observations of the plastic zone in thin polymer films tests in EWF method. As the thickness over notch radius ratio $t/R \geq 4$, we observe at the center of the specimen the development of shear bands similar to those predicted by Lai and Van der Giessen [1] who performed 2D plane strain calculations, for a mode I load. These observations can be used to estimate the region where plane stress and plane strain prevail. In particular, it can be used as an indicator to assess whether or not plane strain conditions are dominant. Actually, for the case with $t/R=16$ (4mm thickness specimen), plane strain conditions with characteristic shear bands are observed, similarly to those predicted by Lai and Van der Giessen [1] and observed experimentally (Ishikawa et al. [13] for instance). For this series of calculations, plane stress conditions prevail for $t/R < 4$, plane strain effects emerge for $t/R=4$ and these conditions become dominant when $t/R > 4$, as shown for the case with $t/R=16$.

On the other hand, the case corresponding to plane strain conditions exhibits the largest magnitude of the maximum mean stress for a given loading. This case is investigated in detail in Lai and Van der Giessen [1] who evidenced that the location of the maximum mean stress coincides with the intersection of well defined shear bands that enhance its magnitude. The plots of the maximum mean stress with loading of the 3D calculations are bounded by those corresponding to the 2D planes stress and 2D plane strain cases. The calculations with thickness $t=1\text{mm}$ ($t/R=1$) results in a plot of the maximum mean stress with loading close to that of the 2D plane stress case. As the thickness increases, the maximum mean stress-loading curve moves from the 2D plane stress to the 2D plane strain case. The shift is clear when carrying from 1mm to 4 mm in thickness and its variations becomes modest for larger thicknesses. The plots reported in Fig. 4 provide insights on whether plane stress or plan strain condition is dominant, for a given thickness to notch radius ratio. The foregoing observation that plane strain conditions become dominant at about $t/R=16$ is confirmed by the analysis of the maximum mean stress during loading. This somehow confirms the qualitative analysis based on the shape of the plastic zone presented in the previous section and evidences the influence of the thickness mean stress constraint in the notch region.

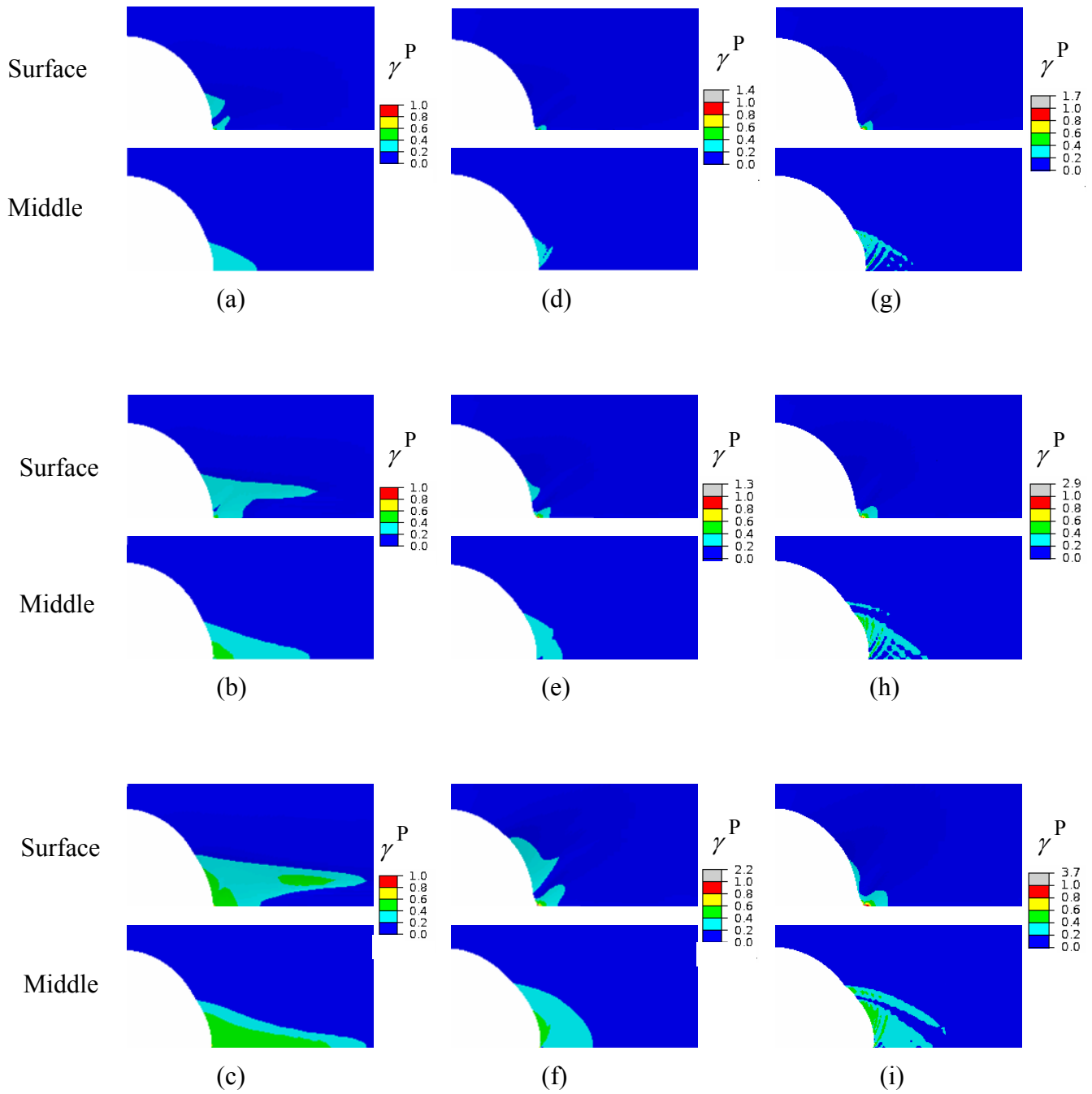


Figure 3. Plastic shear strain distribution at the surface and the mid-thickness, for $R=0.25\text{mm}$, at $E_{\text{axial}}=0.75\%$, 0.875% and 1.125% , (a-c) for $t=0.25\text{mm}$; (d-f) for $t=1\text{mm}$; (g-i) for $t=4\text{mm}$.

4. Discussion and conclusion

The calculations performed in present work allow to compare the plastic zone at the center as well as on the surface of specimens. Plastic shear strain distribution of blunt-notched polymer bulks are reported, corresponding to specimens with various thicknesses and an initial blunted notch $R=0.25\text{mm}$.

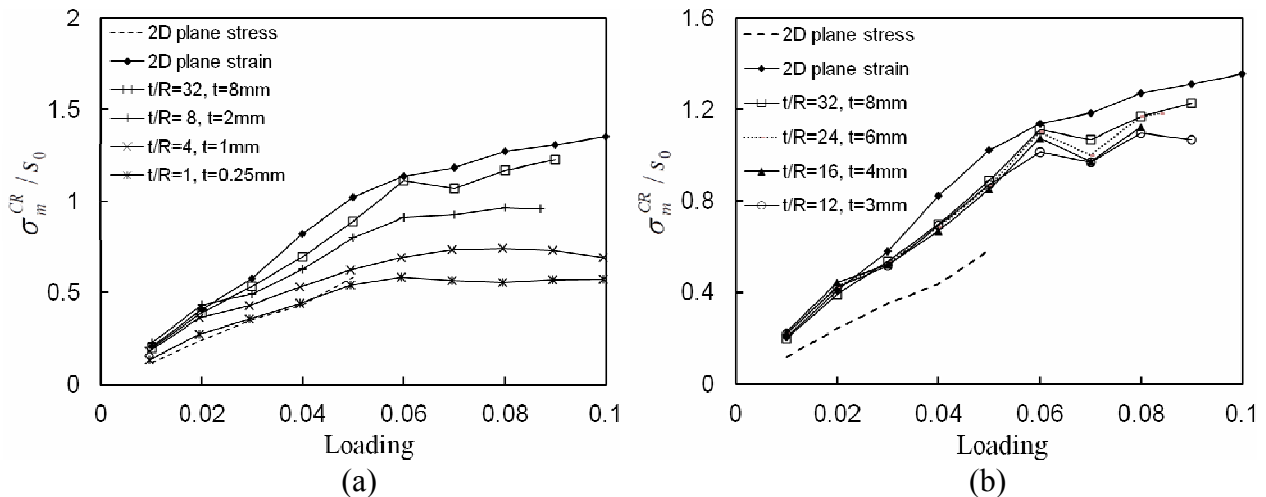


Figure 4. Variation of the maximum mean stress with loading for the 3D specimens of various thicknesses and 2D configurations under plane stress and plane strain conditions ($R=0.25\text{mm}$)

The shape of the plastic zone is shown useful as a marker for identifying if plane stress or plane strain conditions prevail. For the mode I under consideration here, a flame-like plastic contour is observed where plane stress conditions are met, for a small thickness and a ratio $t/R \leq 4$ (thickness/notch radius). The shape of flame-like elongated plastic zone for the specimen with $t/R=1$ is in agreement with Hashemi's observations reported in [2]. By increasing the thickness and the ratio t/R , the shape of the plastic zone evolves from the flame-like to a plastic strain distribution. As for specimens with $t/R=16$, typical shear bands appear at the center of polymer, which are similar to that observed in Hill's slip line field and comparable to that reported by Lai and Van der Giessen[1]. The onset of a transition from plane stress or plane strain condition is observed as soon as the ratio thickness/notch radius $t/R=4$. This observation is consistent with that reported by Parvin and Williams [3], if one considers the radius of the blunt crack $R_p \approx R$ is ductile polymer with a blunt notch. Thus, we propose a criterion to distinguish between plane stress and plane strain conditions. Although the criterion $t/R > 4$ for plane strain conditions to emerge is established to $R=0.25\text{mm}$, we have investigated samples with a smaller (0.1mm) and a larger (0.5mm) notch radius. The variations of the plastic zone shape with the ratios t/R reported in Fig. 3 are also observed for $R=0.1\text{mm}$ and $R=0.5\text{mm}$. This observation appears valuable when one considers an initial blunt notch.

For the configuration with an initial sharp crack, the onset of failure is usually taken from a Crack Tip Opening Displacement that is measurable experimentally. The CTOD is the characteristic of the material under consideration and its magnitude could be used as the value of the blunted notch radius and compare to the thickness in order to evaluate the minimum thickness for plane strain conditions. This information is valuable for one concerns with experimental polymer fracture and the issue of the size requirements for the estimation of the material's toughness. The present predictions need to be compared to experimental results. This is currently under progress and some preliminary results can already be reported. We have prepared the samples depicted in Figure 2 and performed some SENT fracture tests. In figure 5, we report the variation of the stress at rupture with the thickness. All samples have the same geometry in terms of crack length versus specimen width and the same height. In Fig. 5, we observe that the stress at rupture decreases with the thickness increasing with a plateau being reached for $t/R=16$. These first results are consistent with the predictions found here as the lowest stress at fracture is found for a specimen thickness larger than 4mm. A more detailed experimental investigation is under progress and will be addressed in a forthcoming paper.

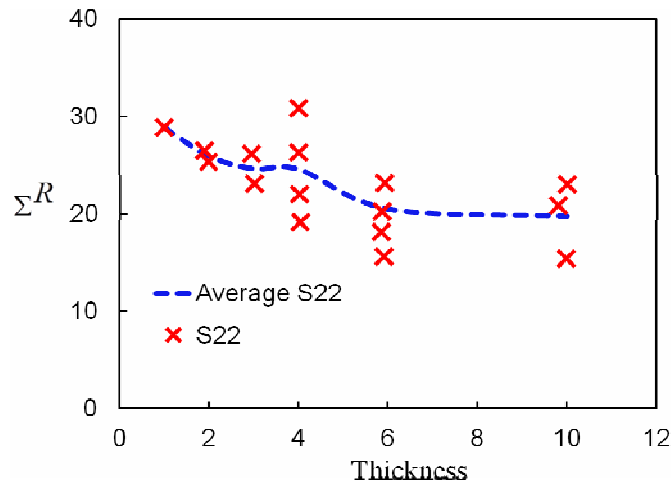


Figure 5. Experimental investigation of the stress at rupture from SENT specimen identical to those depicted in Fig. 2

Acknowledgements

This research program is supported by CSC(China Scholarship Council) in collaboration with INSA Lyon.

References

- [1] J.Lai, E. der Giessen, A numerical study of crack-tip plasticity in glassy polymers, *Mechanics of Materials*, 25 (1997) 183–197.
- [2] S. Hashemi, Plane-stress fracture of polycarbonate films, *Journal of Materials Science*, 28 (1993) 6178–6184.
- [3] M. Parvin, J. Williams, Ductile-brittle fracture transitions in polycarbonate, *International Journal of Fracture*, 11 (1975) 963–972.
- [4] V. Tvergaard, A. Needleman, An analysis of thickness effects in the izod test, *International Journal of Solids and Structures*, 45 (2008) 3951–3966.
- [5] M.C. Boyce, D.M. Parks, A.S. Argon, Large inelastic deformation of glassy polymers, part I rate dependent constitutive model, *Mechanics of Materials*, (1988) 15–33
- [6] P. D. Wu, E. der Giessen, On improved network models for rubber elasticity and their applications to orientation hardening in glassy polymers, *Journal of the Mechanics and Physics of Solids*, 41 (1993) 427–456.
- [7] P. D. Wu, E. van der Giessen, Computational aspects of localized deformation in amorphous glassy polymers, *European Journal of Mechanics., A/Solids*, 15 (1996) 799–823.
- [8] Abaqus finite element package, v. 6.10, Simulia, Dassault Systems.
- [9] A. S. Argon, A theory for the low-temperature plastic deformation of glassy polymers, *Philosophical Magazine*, 28 (1973) 839–865.
- [10] P. D. Wu, E. der Giessen, On improved network models for rubber elasticity and their applications to orientation hardening in glassy polymers, *Journal of the Mechanics and Physics of Solids*, 41 (1993) 427–456.
- [11] E. M. Arruda, M. C. Boyce, A three-dimensional constitutive model for the large stretch behavior of rubber elastic materials, *Journal of Physics and Solids*, 41(1993) 389–412.
- [12] N.Saad-Gouider, R.Estevez, C.Olagnon, R.Séguéla, Calibration of a viscoplastic cohesive zone for crazing PMMA, *Engineering Fracture Mechanics*, 73 (2006) 2503–2522.
- [13] M. Ishikawa, I. Narisawa, H. Ogawa, Criterion for craze nucleation in polycarbonate, *Journal of Polymer Science: Polymer Physics Edition*, 15 (1977) 1791–1804.